



HAL
open science

Homoleptic Co II , Ni II , Cu II , and Zn II Complexes Based on 8-Hydroxylquinoline Schiff Base Derivative: a Combined Synthetic, Spectral, Structural, and Magnetic Study

Déborah González, Ramon Arrue, Edison Matamala-Cea, Rodrigo Arancibia, Paul Hamon, Olivier Cador, Thierry Roisnel, Jean-René Hamon, Néstor Novoa

► To cite this version:

Déborah González, Ramon Arrue, Edison Matamala-Cea, Rodrigo Arancibia, Paul Hamon, et al.. Homoleptic Co II , Ni II , Cu II , and Zn II Complexes Based on 8-Hydroxylquinoline Schiff Base Derivative: a Combined Synthetic, Spectral, Structural, and Magnetic Study. *European Journal of Inorganic Chemistry*, 2018, 2018 (43), pp.4720-4730. 10.1002/ejic.201801160 . hal-01945150

HAL Id: hal-01945150

<https://univ-rennes.hal.science/hal-01945150>

Submitted on 5 Dec 2018

HAL is a multi-disciplinary open access archive for the deposit and dissemination of scientific research documents, whether they are published or not. The documents may come from teaching and research institutions in France or abroad, or from public or private research centers.

L'archive ouverte pluridisciplinaire **HAL**, est destinée au dépôt et à la diffusion de documents scientifiques de niveau recherche, publiés ou non, émanant des établissements d'enseignement et de recherche français ou étrangers, des laboratoires publics ou privés.

Homoleptic Co(II), Ni(II), Cu(II), and Zn(II) complexes based on 8-hydroxyquinoline Schiff base derivative: a combined synthetic, spectral, structural, and magnetic study[†]

Déborah González,^[a] Ramón Arrué,^[a] Edison Matamala-Cea,^[a] Rodrigo Arancibia,^[a] Paul Hamon,^[b] Olivier Cador,^[b] Thierry Roisnel,^[b] Jean-René Hamon*,^[b] and Néstor Novoa*^[a]

[a] *Laboratorio de Química Inorgánica y Organometálica, Departamento de Química Analítica e Inorgánica, Facultad de Ciencias Químicas, Universidad de Concepción, Edmundo Larenas 129, Casilla 160-C, Concepción, Chile.*
E-mail: nenovoa@udec.cl

[b] *Univ Rennes, CNRS, ISCR (Institut des Sciences Chimiques de Rennes) – UMR 6226, F-35000 Rennes, France.*
E-mail: jean-rene.hamon@univ-rennes1.fr

Dedicated to the memory of our esteemed colleague Dr. Jean-Yves Pivan (ENSC Rennes), an enthusiastic chemist and brilliant supervisor.

[†]Supporting information and ORCID(s) from the author(s) for this article are available on the WWW under <https://doi.org/10.1002/ejic.201801160>.

Abstract: A series of four new homoleptic Co(II), Ni(II), Cu(II) and Zn(II) complexes (**1-4**) of the type $M(HL)_2$, where HL^- stands for the deprotonated form of the tridentate O,N,N-donor Schiff base ligand obtained by condensation between 8-hydroxy-2-quinolinecarboxaldehyde and 2-aminophenol, have been prepared in yields ranging from 70 to 85%. The five compounds were characterized using elemental analysis, FT-IR, ESI-MS, UV-Vis, and 1H & ^{13}C NMR spectroscopies (for the diamagnetic species H_2L and Zn(II) complex **4**). The molecular structures of H_2L and its Ni(II) and Zn(II) complexes **2** and **4**, respectively, were further confirmed by single crystal X-ray diffraction methods. X-ray crystal structure determination revealed that in complex **2**, the six-coordinate Ni(II) metal ion adopts a N_4O_2 distorted octahedral geometry with the two tridentate HL^- ligands coordinated in a perfect orthogonal fashion. In complex **4**, however, the Zn(II) metal center is pentacoordinated and lies in a distorted N_3O_2 trigonal bipyramidal environment, one HL^- ligand acting as an O,N-bidentate ligand. In both cases, a free hydroxyl unit remains available for supramolecular interactions. Hirshfeld surface (HS) analysis along with 2D fingerprint plots were employed to consider the intermolecular forces, including hydrogen bonds and $\pi-\pi$ stacking interactions, and their quantification in the crystal lattice. SQUID magnetometry experiments showed high spin Co(II) ($S = 3/2$), Ni(II) ($S = 1$) and Cu(II) ($S = 1/2$) isolated spins at room temperature with no interaction between magnetic centers on cooling.

Introduction

Schiff bases are ubiquitous ligands facilely synthesized and coordinated to almost all the metal ions, thus creating a very fertile and dynamic research field in coordination chemistry.^[1-6] They are readily formed upon condensation reactions of a primary amine with a carbonyl group, and are characterized by an imine ($>C=N-$) or azomethine ($-HC=N-$) function. Due to their highly modular synthesis allowing the control of the nature of donor atoms, chelating ability, as well as their electronic and steric properties, Schiff base ligands can readily form stable complexes with most of the transition metals in various oxidation states and multiple forms of coordination towards the metallic ions.^[7,8] Consequently, Schiff base complexes have found applications in different branches of science such as catalysis,^[9-12] magnetism,^[13-15] sensing,^[16,17] optical,^[18,19] and energy sciences,^[20] as well as medicinal chemistry.^[21,22]

Among the Schiff bases, N_2O_2 tetradentate based salen-type ligands where H_2 -salen (N,N-bis(salicylidene)ethylenediamine) is the quintessential representative of this class of symmetrical di-imines compounds,^[23] continue to be the most popular and the most studied ones.^[17,24] They are generally prepared in high yields by condensation of any primary diamine with two equivalents of salicylaldehyde derivatives.^[1,25] Mono-condensed Schiff bases have also been obtained either by direct,^[26,27] or metal template,^[28,29] reactions between carbonyl units and appropriate amino alcohol, diamine or aminothiols substrates, yielding a large variety of tridentate ligands featuring ONX-donor sets ($X = O, N,$ and S).^[7,30-33] Metal complexes prepared with these ligands show diverse structure features, topology, nuclearity as well as supramolecular architectures, depending on the experimental conditions (metal-to-ligand ratios, supporting anions, solvents, etc).^[3,7,34-36] At this stage, it is worthy to emphasize that ONN-tridentate derivatives bearing a pendant free amino group are useful building blocks for the synthesis of unsymmetrically-substituted tetradentate and compartmental Schiff base ligands.^[7,37]

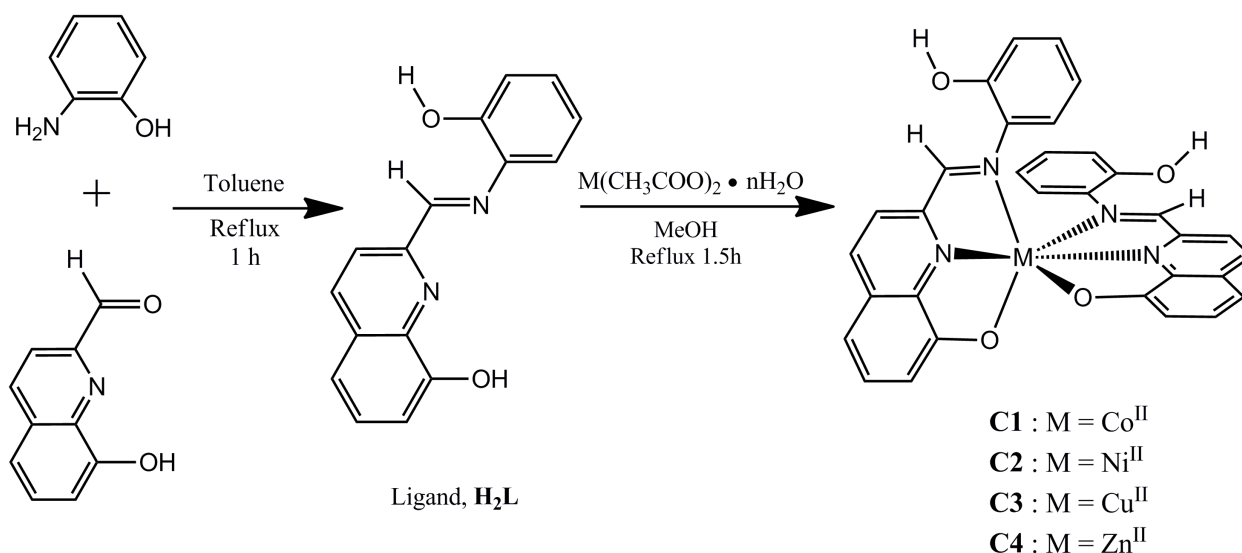
In the tridentate ONX-type family, albeit much less well developed, quinoline salicylaldimine based ligands^[38,39] have been investigated for their versatility towards various transition metal with interesting structural, biological, optical, magnetic and catalytic properties.^[40-51] The tridentate quinoline Schiff bases act as planar monoanionic ligands incorporating the pyridine moiety and exhibiting an extended π -system. The fused aromatic rings provide a rather rigid skeleton that enforces a meridional configuration at the metal center. The most studied ones result from condensation of aminoquinoline with

salicylaldehyde producing variously substituted ((quinolinyl-imino)methyl)phenol derivatives.^[38,39] 8-hydroxyquinoline based Schiff bases are less common. 5-amino substituted 8-hydroxyquinoline derivatives were recently used by Cui and co-workers to prepare a series of tetranuclear lanthanide complexes, some of them featuring magneto-caloric effect and slow magnetic relaxation (SMM) behavior.^[52,53] In 1972, Hata and Uno reported the synthesis of N-2-(8-hydroxyquinolin-2-ylazomethine)phenol (**H₂L**, Scheme 1) obtained by Schiff condensation of 8-hydroxyquinoline-2-carbaldehyde with 2-aminophenol.^[54] Interestingly, this ONN tridentate quinoline Schiff base ligand possesses a pendant hydroxyl group which could, as observed in the salicylidene-(2-hydroxyethyl)imine series, generate weak noncovalent interactions leading to the formation of extended supramolecular structures,^[33,55] or engage into coordination with a neighbouring metal center to form one-dimensional coordination polymeric chains.^[56] In the present work, four new homoleptic metal(II) complexes [M(HL)₂] (M = Co, **1**; Ni, **2**; Cu, **3**; Zn, **4**) derived from HL ligand, the monodeprotonated form of the diprotic **H₂L** Schiff base precursor, have been synthesized and characterized. The structures of the pro-ligand **H₂L** and of the Ni(II) and Zn(II) complexes have been confirmed by single crystal X-ray crystallographic analysis. Solid-state supramolecular interactions of the three compounds have also been described; Hirshfeld surface (HS) analysis along with 2D fingerprint plots were used to quantify intermolecular forces. Furthermore, magnetic properties of the paramagnetic complexes **1-3** were investigated.

Results and discussion

Synthesis and some properties of ligand precursor **H₂L** and metal(II) complexes **1-4**.

The known diprotic Schiff-base ligand N-(8-Hydroxyl-2-quinolylmethylene)-*o*-aminophenol (**H₂L**) only characterized by its melting point and elemental analysis,^[54] was synthesized following a slightly modified procedure. **H₂L** was, indeed, formed upon reacting equimolar amount of 8-hydroxyquinoline-2-carbaldehyde and 2-aminophenol in refluxing toluene for 1 h (Scheme 1). It was isolated as a yellowish powder in 97% crude yield upon cooling the reaction mixture to room temp. Recrystallization from dichloromethane afforded a yellow microcrystalline solid (see Exp. Sect.).



Scheme 1. Synthesis of the diprotic ligand **H₂L** and its metal(II) complexes **1-4**.

The neutral complexes **1-4** were straightforwardly obtained by reacting the diprotic Schiff-base precursor **H₂L** with the appropriate hydrated metal(II) acetate salt (2:1 molar ratio), in refluxing methanol for 1.5 h (Scheme 1). The four metal(II) complexes were obtained in moderate to good yield (60-84%) and isolated as microcrystalline dark solids. The Schiff-base proligand **H₂L** as well as its four respective coordination compounds **1-4** are air and thermally stable, and moisture insensitive on storage under ordinary condition. They exhibit good solubility in common polar organic solvents but are not soluble in diethyl ether and hydrocarbon solvents. Complexes **1-4** having two uncoordinated phenol groups are soluble in buffered water (pH = 9.0, 25 °C). Under more basic conditions (pH = 14, NaOH), they start to decompose after a few minutes. Satisfactory elemental analysis, FT-IR, ¹H and ¹³C NMR (only for **H₂L** and **4**, see Supporting Information), UV-Vis spectroscopy, and single-crystal X-ray diffraction study (for **H₂L**, **2** and **4**) helped to confirm their purity, composition and identity. In addition, complexes **1-4** were characterized by their respective molecular ion peak [M]⁺ or as the sodium aggregate [M+Na]⁺ in their HRMS-ESI (positive mode) mass spectra (see Exp. Sect.).

Spectroscopic characterization

The solid-state FT-IR spectra of complexes **1-4** exhibited similar absorption band patterns suggesting the analogy of their molecular structures. They reveal the disappearance of the quinolinic O-H stretching vibrations observed in the spectra of the ligand precursor **H₂L** at 3413 cm⁻¹, whereas bands in the range 3367 – 3371 cm⁻¹ attributed to the *o*-phenylene O-H

stretching vibrations of the free ligand **H₂L** remained. In addition, a bathochromic shift of 27-31 cm⁻¹ of the C=N stretching vibration of the azomethine group found at 1616 cm⁻¹ in the free **H₂L** pro-ligand is observed upon complex formation. Such observations indicate that the chelating Schiff base ligand is bonded to the metal(II) ion in its mono-anionic form and in a tridentate fashion through the O,N,N⁻ donor set (O-Phenolic, N-Pyridine and N-imine). Thus, complexes **1-4** adopt a M(HL)₂-type structure where each HL ligand bears a free *o*-phenylene hydroxyl group.

The electronic absorption spectra in the UV-Vis region of the free **H₂L** and its corresponding complexes **1-4** were recorded in DMSO solution at room temperature. The experimental spectra of **H₂L**, **2** and **4** are shown in Figure 1, while the deconvoluted ones are displayed with those of **1** and **3** in Figures S1 and S2 (Supporting Information), respectively. The deconvoluted spectral data are gathered in Table 1. The high energy absorption bands at 272 nm (for **H₂L**) and in the 289-304 nm range (for **1-4**) may be assigned as intraligand π - π^* charge transfer (ILCT) transition, and relatively lower energy absorption peaks at 365 nm (for **H₂L**) and in the 349-355 nm range (for **1-4**) may be ascribed to the ligand centered n - π^* transition. The observed hypsochromic shift associated with the decrease in intensity of the absorption bands (Table 1) may be attributed to the coordination of the HL⁻ ligand heteroatoms to the metal center. Complexes **1-4** displayed absorptions around 380 nm and shoulder in the 445-498 nm range, which is consistent with ligand to metal charge transfer (LMCT) transitions. Similar results were found for other bis-(tridentate Schiff base) late first-row transition metal complexes,^[33,45,57,58] suggesting that the octahedral geometry around the metal(II) core is preserved in DMSO solution. It was further confirmed with X-ray crystal structure analysis, at least in the case of the Ni(II) derivative **2** (see below). In addition, a weak absorption band due to *d-d* transition appeared at 602 nm for the Cu(II) complex **3**.^[35,59]

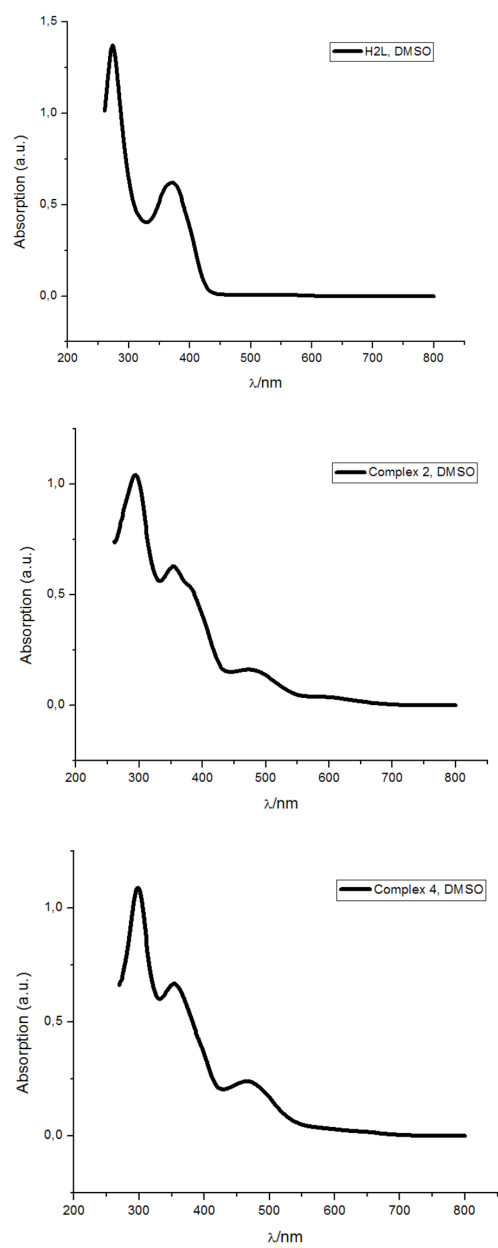


Figure 1. Experimental UV-Vis spectra of **H₂L** (top), **2** (middle) and **4** (bottom), recorded in DMSO at room temp.

Table 1. Electronic spectral data for compounds **H₂L** and **1-4**^[a]

Compound	Band	λ/nm (log ϵ)
H₂L	A	272 (4.44)
	B	365 (4.13)
1	A	296 (4.36)
	B	349 (3.96)
	C	378 (3.97)
	D	463 (3.72)
2	A	304 (4.30)
	B	355 (3.96)
	C	383 (3.81)
	D	498 (3.46)
3	A	289 (4.35)
	B	351 (3.80)
	C	383 (4.02)
	D	472 (3.56)
	E	602 (2.87)
4	A	296 (4.34)
	B	350 (3.85)
	C	380 (3.88)
	D	445 (3.62)

[a] Spectra recorded in DMSO at room temp.

Description of the X-ray crystal structures

Single crystals suitable for X-ray structure investigation were obtained for the ligand precursor **H₂L** and its Ni(II) and Zn(II) complexes **2** and **4**, respectively, by either slow evaporation or vapor diffusion techniques (see Exp. Sect). The molecular structure of **H₂L** is displayed in Figure 2 with selected bond distances and angles given in the caption. Those of **2** and **4** are depicted in Figures 3 and 4, respectively. Selected bond lengths and angles of the first metal(II) coordination sphere of **2** and **4** are given in Table 2, while those of the HL⁻ ligands of the two complexes are provided in Table S1 (Supporting Information). The ligand precursor **H₂L** crystallizes in the non-centrosymmetric space group $P2_1$, whereas complexes **2** and **4** crystallize in the centrosymmetric space groups $P-1$ and $P2_1/n$, respectively, with in all the three cases one molecule per asymmetric unit. The single-crystal X-ray diffraction studies confirm the formation of the ligand precursor **H₂L** through a Schiff base condensation between 8-hydroxylquinoline-2-carbaldehyde and 2-aminophenol, and that both **2** and **4** are neutral species in which the two tridentated anionic monodeprotonated HL⁻ ligand adopts a meridional coordination mode. Such a “mer” coordination type presumably favors the flatness of the ligand with an extended π -delocalization that would probably be preferred over a more constraint facial arrangement. The other aspects of the structures are discussed below in three sections for the sake of simplicity.

Ligand precursor H₂L. The molecular structure reveals an almost planar Schiff base molecule with a dihedral angle of 10.8° between the planes of the pendant phenol and quinoyl rings (Figure 2). Proligand H₂L Adopts an *E*-conformation,^[27] with respect to the C=N double bond. The azomethine C=N bond distance (1.295(7), Å) is similar to those previously measured for structurally related Ar-C(H)=N-Ar Schiff base compounds.^[60-62] The metric parameters observed in the aromatic cycles reveal a strong delocalization throughout the π -system, with average C-C bond lengths of 1.382 Å, 1.395 Å, and 1.398 Å, for the *o*-phenylene, fused C₆ and pyridine rings, respectively. In the 8-hydroxylquinoyl fragment, intramolecular hydrogen bonding between the hydroxyl hydrogen and the nitrogen of the pyridinic ring is observed with an O(2)⋯N(2) separation of 2.698(7) Å.

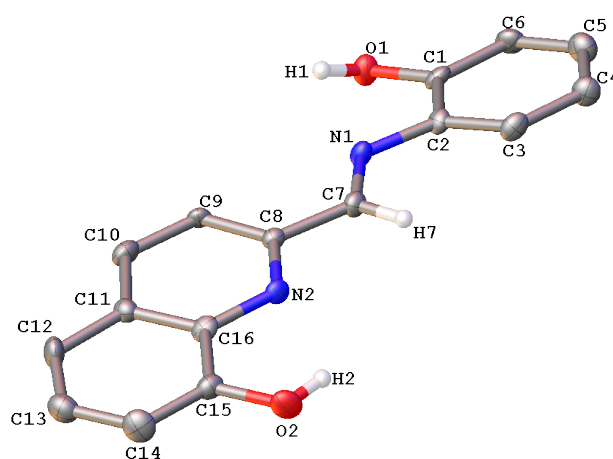


Figure 2. Molecular structure of ligand precursor H₂L with partial atom labelling scheme. Hydrogen atoms have been omitted for clarity. Thermal ellipsoids are drawn at 40% probability. Selected bond lengths [Å] and angles [°]: O(1)-C(1) 1.351(7), C(1)-C(2) 1.402(8), N(1)-C(2) 1.397(9), N(1)-C(7) 1.295(7), C(7)-C(8) 1.461(9), N(2)-C(8) 1.339(7), N(2)-C(16) 1.354(8), C(15)-C(16) 1.417(8), O(2)-C(15) 1.363(8); O(1)-C(1)-C(2) 120.60(6), N(1)-C(2)-C(1) 114.10(5), C(2)-N(1)-C(7) 120.90(5), N(1)-C(7)-C(8) 121.10(5), N(2)-C(8)-C(7) 114.30(5), N(2)-C(16)-C(15) 116.80(5), C(8)-N(2)-C(16) 117.50(5), O(2)-C(15)-C(16) 119.40(6).

Complex 2. Compound 2 appears to be a neutral mononuclear distorted octahedral nickel(II) species with a N₄O₂ donor atoms set (Figure 3). The *pseudo*-octahedral coordination environment has nitrogen N(1) and oxygen O(2) atoms in apical positions while the three nitrogen (N(2), N(3), and N(4)) and the oxygen O(4) atoms define the basal plane and lie -

0.0729(5), +0.0923(7), -0.1189(9), and +0.0995(8)Å, respectively, out of the least-squares plane through them. The Ni atom lies +0.0567(8)Å out of this LS plane in the direction of the apical N(1) atom. The two mono-anionic ligands HL⁻ coordinate meridionally in a terdentate (O-Phenolic, N-Pyridine and N-imine) fashion to the central Ni(II) ion. The two pyridine nitrogen atoms N(2) and N(4) are mutually *trans*, while the two imine nitrogen N(1), N(3), and the two phenolic O(2), O(4) oxygen atoms are mutually *cis*. The two tridentate HL⁻ ligands are individually essentially planar and are coordinated in a perfect orthogonal fashion (dihedral angle = 90.1°) to the central nickel(II) metal ion. Two five-membered heterometallacycles are formed by each tridentate ligand upon complexation to the metal center. The two types of chelate bite angles (N-Ni-N and O-Ni-N) formed around the nickel(II) ion, by the imine-N and quinolyl-N atoms (76.02(6)° and 75.68(6)°) are slightly smaller than those formed by phenoxo-O and quinolyl-N ones (79.46(6)° and 79.29(6)°), Suggesting a better chelation in the former rings. This might be accounted for by a greater flexibility of the azomethine unit compared to the rigid structure of the hydroxoquinolyl fragment.

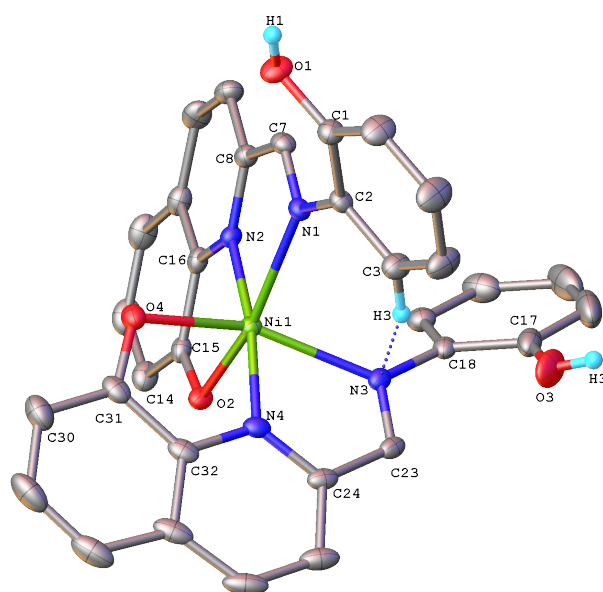


Figure 3. Molecular structures of nickel(II) complex **2**, showing a partial atom-numbering scheme. Hydrogen atoms are omitted for clarity. Thermal ellipsoids are drawn at 40% probability.

The distortion from ideal octahedral coordination geometry at the metal center is markedly noticeable with mean deviations from ideal angles (90° and 180°) of 7.525° and

19.85°, and with maximum deviations of 14.33 ° and 25.41°, respectively (Table 2). Those significant deviations from the idealized values could be due to the rigidity of the coordinated planar ligands, as previously observed for distorted octahedral Ni(II) complexes featuring a N₄O₂ donor set.^[45,46,57,63] The Ni(II)-N bond distances vary from 1.9657(15) to 2.2393(15) Å (Table 2) with the bond to the imine nitrogen significantly longer than that of the quinolyl nitrogen by 0.26 Å. The Ni(II)-O bond lengths are 2.1144(12) and 2.1195(14) Å, the equatorial distance being barely shorter than the axial one.

Table 2. Selected bond distances[Å] and angles[°] for the first metal(II) coordination sphere of compounds **2** and **4**.

	2	4
Bond distances		
M(1)-O(2)	2.1144(12)	2.110(4)
M(1)-O(4)	2.1195(14)	1.996(4)
M(1)-N(1)	2.2393(15)	2.391(5)
M(1)-N(2)	1.9657(15)	2.005(4)
M(1)-N(3)	2.2225(15)	-
M(1)-N(4)	1.9728(16)	2.039(5)
Bond angles		
N(2)-M(1)-N(4)	170.50(6)	143.00(2)
N(1)-M(1)-O(2)	155.36(5)	151.28(16)
N(3)-M(1)-O(4)	154.59(6)	-
N(2)-M(1)-O(2)	79.46(6)	79.15(17)
N(2)-M(1)-N(1)	76.02(6)	73.97(18)
N(4)-M(1)-O(4)	79.29(6)	82.80(2)
N(4)-M(1)-N(3)	75.66(6)	-
N(1)-M(1)-N(3)	94.11(5)	-
N(1)-M(1)-N(4)	112.86(6)	113.97(17)
N(1)-M(1)-O(4)	91.57(5)	90.75(16)
N(2)-M(1)-N(3)	107.86(6)	-
N(2)-M(1)-O(4)	97.55(6)	134.16(18)
O(2)-M(1)-N(3)	91.08(5)	-
O(2)-M(1)-N(4)	91.57(5)	93.60(17)
O(2)-M(1)-O(4)	93.99(5)	100.99(16)

M = Ni for **2**, and Zn for **4**.

Complex 4. The molecular structure of **4** (Figure 4), shows that the complex consists of two mono-anionic HL⁻ ligands coordinating to the zinc(II) ion, one in a meridionally tridentate fashion through the O-Phenolic, N-quinolyl and N-imine atoms, and the other one in a bidentate mode through the O,N-donor atoms set of the hydroxyquinolyl fragment, to afford a five-coordinate geometry. Zn(II) is therefore sitting in a N₃O₂ coordination environment from the two Schiff base ligands that define a distorted trigonal bipyramidal geometry about the metal ion. Thus, the two O-Zn-N chelate bite angles are different: O(2)-Zn(1)-N(2) = 79.15(17)° is similar to the corresponding angle measured in the Ni(II) complex **2** (see

above), whereas O(4)-Zn(1)-N(4) of $82.80(2)^\circ$ is slightly greater. This could arise from the bidentate coordination of the second HL⁻ ligand by releasing of steric strain, highlighting the flexibility of the HL⁻ ligand. In the above mentioned description, The axial sites are occupied by the N(1) and O(2) atoms, while the trigonal plane is defined by the N(2), N(4), and O(4) atoms, with the Zn atom located $0.024(4)$ Å out of this plane in the direction of O(2) atom. Distortion of the coordination sphere around the Zn(II) metal center from the ideal trigonal bipyramidal geometry, is manifested in: (i) the N(1)-Zn(1)-O(2) angle of $151.28(16)^\circ$ which reflects the restricted bite angle of the ligand; (ii) the three equatorial angles ranging from $82.80(2)^\circ$ to $143.00(2)^\circ$; and (iii) the axial-Zn(1)-equatorial angles comprised between $73.97(18)^\circ$ and $113.97(17)^\circ$ (Table 2). Such distorted geometry has already been encountered for pentacoordinated Zn(II) species.^[64] The Zn-N bond distances of the basal plane ($2.005(4)$ and $2.039(5)$ Å) are much shorter than the axial one ($2.391(5)$ Å). This is also true for the Zn-O bond lengths (Table 2). Moreover, a short contact ($2.722(4)$ Å) exists between the metal ion and the azomethine nitrogen N(3) of the bidentate ligand (Figure 4). Interestingly, although in the crystal structure of **4** the two ligands are not equivalent, in solution the molecular structure is symmetric as established by ¹H and ¹³C NMR spectra showing a single set of signals for the two equivalent ligands (see above and Exp. Sect.). A fast equilibrium on the NMR timescale involving the decoordination/coordination of the two iminic nitrogen atoms does presumably occur in solution.

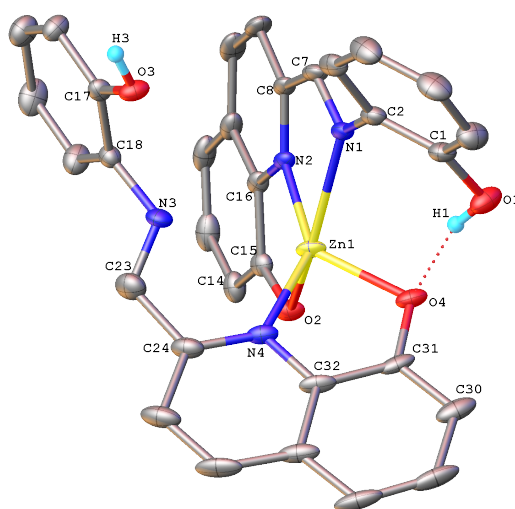


Figure 4. Molecular structures of the Zinc(II) compound **4**, showing a partial atom numbering scheme and the intramolecular H-bond O(1)H \cdots O(4). Hydrogen atoms are omitted for clarity with exception of hydroxilic H atoms. Thermal ellipsoids are drawn at 20% probability.

Solid-state supramolecular interactions

The molecules of **H₂L** are connected through a series of intermolecular hydrogen bonds (Table 3, and Figure S3 (Supporting Information)). The projection of the packing shows an extended parallel-displaced disposition, possibly attributable to the π -stacking interactions between the aromatic systems and the nitrogen atoms (Table 3, and Figure S4 (Supporting Information)) due to an intermolecular close contact involving the two rings (Cg₂-Cg₃) of the quinolic fragment of each molecule. In addition, this arrangement can be explained by the hydrogen bonds formed beside parallel-displaced molecular-chains (see Figure S3 (Supporting Information)).

Table 3. Close contact interactions in **H₂L** and its complexes **2** and **4**.

Hydrogen bond calculated by X-ray diffraction					
<i>Donor-H ... Acceptor</i>	<i>D-H(Å)</i>	<i>H ... A(Å)</i>	<i>D ... A(Å)</i>	<i>D-H ... A(°)</i>	
Ligand H₂L					
O(1)-H(1) ... O(1) ^[a]	0.84	2.169	2.962	145.3	
C(9)-H(9) ... O(1) ^[a]	0.95	2.440	3.386	174.3	
C(3)-H(3) ... O(2) ^[a]	0.88	2.492	3.439	174.4	
C(14)-H(14) ... O(2) ^[a]	0.95	2.492	3.339	174.4	
C(4)-H(4) ... O(2) ^[a]	0.95	2.776	3.370	121.4	
C(5)-H(5) ... O(2) ^[a]	0.95	2.632	3.305	128.3	
Complex 2					
O(1)-H(1) ... O(4) ^[a]	0.83	1.790	2.618	175.76	
C(6)-H(6) ... O(2) ^[a]	0.95	2.654	3.319	127.48	
C(9)-H(9) ... O(2) ^[a]	0.95	2.568	3.445	153.72	
C(4)-H(4) ... O(1) ^[a]	0.95	2.643	3.439	141.72	
C(3)-H(3) ... N(3) ^[b]	0.95	2.636	3.478	147.93	
Complex 4					
O(3)-H(3) ... O(2) ^a	0.84	1.769	2.600	170.16	
O(1)-H(1) ... O(4) ^b	0.84	1.745	2.558	162.24	
π-π stacking interactions determine by X-ray diffraction					
<i>Centroid-Centroid</i>	<i>Distance(Å)</i>		<i>angle(°)</i>		
Ligand H₂L					
Cg ₂ -Cg ₃ ^[a]	3.946		1.00		
Complex 2					
Cg ₃ -Cg ₃ ^[a]	3.541		0.00		
Complex 4					
Cg ₂ -Cg ₃ ^[a]	3.845		3.18		
Cg ₁ -Cg ₂ ^[a]	3.748		18.36		

[a] neighboring molecule; [b] intramolecular H-bond; where: Cg₁ = C1-C6; Cg₂ = C7(N8)-C9; Cg₃ = C11-C16.

On the other hand, within the crystal packing of nickel(II) derivative **2**, intermolecular O-H...O hydrogen bonds (Table 3) generate a virtual infinite chain-type structure (Figure S5,

Supporting Information). These interactions occur between the hydroxyl hydrogen of each phenolic fragment with the phenolic group of the neighbouring complex. In this regard, the packing of **2** shows the presence of an intramolecular H-bond between C(3)-H (phenolic ring) and the coordinated atom N(1). In addition, the analysis of the intermolecular π - π stacking interactions between Cg₃-Cg₃ rings (Figure S6, Supporting Information) determines the layout of the molecular network in the crystal lattice (Table 3).

Finally, the analysis of the molecular and crystal structure of the zinc(II) complex **4**, reveals the presence of two hydrogen bonds specifically centred in the hydroxyl fragments containing in each molecule (Table 3, and Figure S7 (Supporting Information)). In particular, the presence of an intramolecular H-bond of different nature with respect to the one found for **2**. In this case, the analysis reveals a hydrogen bond between the OH fragment of the phenolic ring and the oxygen coordinated to the metal-core (second HL⁻ ligand of the same complex). In addition, we detected the presence of two types of π - π stacking interactions between the quinolic and phenolic rings (Figure S8, Supporting Information). These short contact interactions can be responsible of the finale orientation in the crystal lattice, and of the good stability of the resulting single-crystal.

Hirshfeld Surface Analysis (HSA)

The supramolecular interactions observed by X-ray diffraction are, surely, determined by indirect approximations. In this regard, performing HSA is a good way to complement the presence of several intermolecular contacts. This analysis is defined as the electron density boundary surfaces between the molecules in a crystal lattice.^[65] During the mapping, the surfaces are kept transparent for the visualization of various supramolecular interactions responsible for the packing stabilization. The HS of **H₂L** mapped in Figure 5 (top) shows the most important supramolecular interaction centred in the -OH unit (red spots), which highlights the close contact through which the intermolecular interaction in the crystal lattice takes place. The colour intensity can be used for visualizing the strength of the interactions. In this regard, the most important interaction is that exhibited by O-H \cdots O bond between two molecules, over the weaker interactions C-H \cdots O previously described in Table 3.

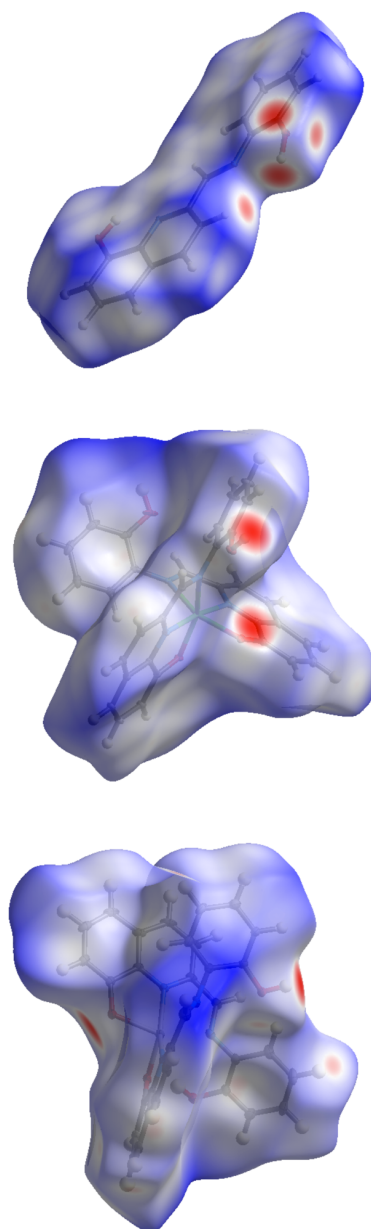


Figure 5. Views of the d_{norm} Hirshfeld surface plotted for **H₂L** (top), **2** (middle), and **4** (bottom). H-bonded are described in Table 3 and text.

In this regard, the analysis of the HS plots obtained for **2** and **4**, shows two important red spots (see Figure 5, middle and bottom), corresponding to O-H \cdots O bonds, and are more important than the present C-H \cdots O interactions previously described in Table 3 (light-red spots). On the other hand, the analysis of the expansion pack considering the most important interactions (red spots), reveals the important role of the hydroxyl fragments in the **H₂L** proligand and its nickel(II) **2** and zinc(II) **4** complexes (Figures S9-S11, Supporting Information). This important supramolecular interaction provides high thermal and moisture

stability (see Exp. Sect.) to the crystal packing, and allows us to project this type of complexes for diverse applications in solid phase. The crucial role of these H-bond interactions can be contrasted by the analysis of the fingerprint plots (Figure 6).

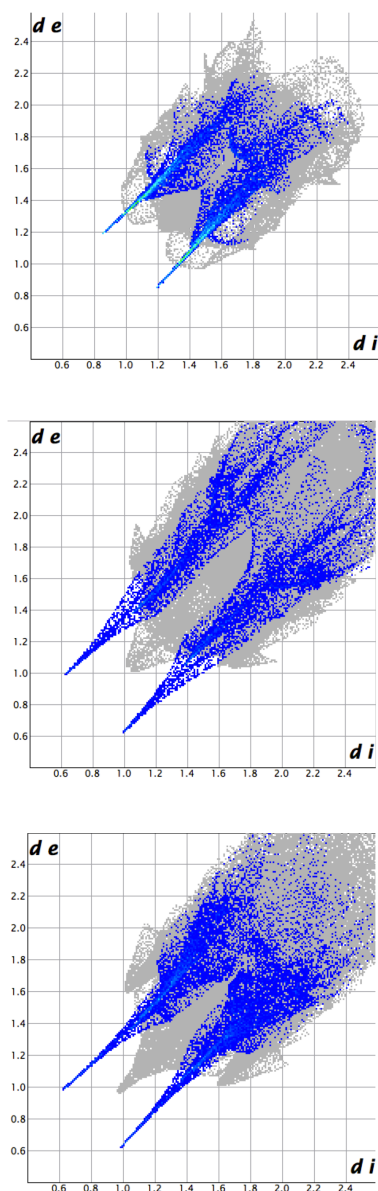


Figure 6. Decomposed fingerprint plots related with HS areas and contributions (including reciprocal contacts) to the total HS for O-H \cdots O hydrogen bonds present in the crystal packing of **H₂L** (top), **2** (middle), and **4** (bottom).

The most relevant O-H \cdots O bonds, present in each crystal packing, represent the following percentage values over the total HS: 14.3, 10.1 and 12.2%, for **H₂L**, **2** and **4**, respectively. In this context, the 2D fingerprint plots are useful in the quantification of

different interactions. The plots of **H₂L** (Figure 6, top) shows the O···H interactions with a shortest $de + di$ distance $\sim 2.17\text{\AA}$, and the 14.3% (including the reciprocal contacts) of the total HS. In addition, the most abundant close contact interaction at long distance is H···H with a 45.2% of the total HS. Finally, the presence of $\pi\cdots\pi$ stacking interactions are evidenced by a light green zone at $de + di \approx 3.60\text{\AA}$ (8.7% C···C + 5.6% C···N) (Figure S12, Supporting Information). The 2D fingerprint plot of **2** (Figure 6, middle) exhibit a shortest $de + di$ distance $\sim 1.84\text{\AA}$, corresponding to the 10.1% (including the reciprocal contacts) of the total HS. In this case, the most abundant close contact interaction at long distance is, also, H···H with a 45.5% of the total HS. Finally, the analysis of the fingerprint plots reveals the weakening of the $\pi\cdots\pi$ stacking interactions on passing from the free ligand to complex **2** (3.3% C···C and 0.0% C···N), probably compensated by the strong H-bond interactions between molecules in the crystal packing (Figure 5, middle). The analysis of the 2D fingerprint plot of the zinc(II) complex **4**, reveals the important and strong intensity of the intermolecular O···H interactions, with 12.2% of the total HS. The plot exhibits a shortest $de + di$ distance $\sim 1.75\text{\AA}$ (Figure 6, bottom), and reveals the high abundance of the H···H interaction in the surface with 51.3% with respect to the total. Considering the other supramolecular interactions, the presence of $\pi\cdots\pi$ stacking arrangement can be attributed in **4** at the most important presences of C···C and C···N close contact in the total HS (5.4% and 1.9%, respectively), compared to the HS of **2**.

Magnetic properties

The magnetization, M , of compounds **1**, **2** and **3** have been measured between 2 and 300 K at two different external magnetic fields: 2 kOe below 20 K and 10 kOe above 20 K. The thermal variation of the magnetic susceptibility is plotted on Figure 7 by means of the $\chi_M T$ product (χ_M being the molar magnetic susceptibility calculated from the ratio M/H , H the magnetic field in Oe and T the temperature in Kelvin). At room temperature, the $\chi_M T$ values for **2** and **3** are equal to 1.27 and 0.39 $\text{cm}^3 \text{K mol}^{-1}$, respectively. These values are in agreement with Ni(II) ($S = 1$) and Cu(II) ($S = \frac{1}{2}$) isolated spins with $g_{\text{Ni}} = 2.25$ and $g_{\text{Cu}} = 2.04$. On cooling $\chi_M T$ remains constant for **3** which indicates that there is no interaction between magnetic centers. For **2**, $\chi_M T$ remains quasi constant down to 25 K. On cooling further $\chi_M T$ decreases continuously down to 0.6 $\text{cm}^3 \text{K mol}^{-1}$ which matches the expected value in the presence of negative Zero Field Splitting (axial local anisotropy).^[66] It also indicates that, like in **3**, there is no interaction between magnetic centers. For **1**, the room temperature value (2.62 $\text{cm}^3 \text{K mol}^{-1}$) is far above the expected value for a spin free $S = 3/2$ with $g = 2$ (1.875 $\text{cm}^3 \text{K mol}^{-1}$). However, owing to the presence of spin orbit coupling important deviations are observed for high spin Co(II).^[66] Also, on cooling, $\chi_M T$ decreases continuously because of the combined effect of the spin orbit coupling and the distortion of the coordination polyhedron, which might be analysed, although inadequate, in a framework of a spin Hamiltonian.^[67] This is, however, beyond the scope of this work.

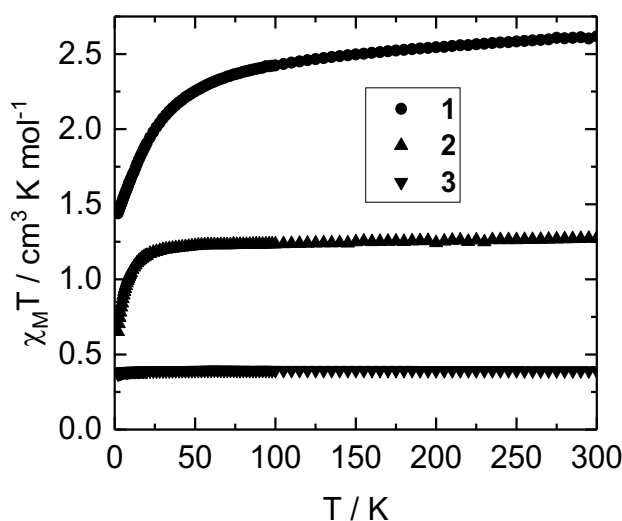


Figure 7. temperature dependences of $\chi_M T$ for the three paramagnetic complexes **1**, **2** and **3**.

Conclusion

In this paper, homoleptic Co(II), Ni(II), Cu(II), and Zn(II) complexes with appended tridentate 8-hydroxyquinoline Schiff base ligand are successfully prepared and characterized by means of various physical methods. Of them, the crystal structure of the Schiff-base ligand precursor **H₂L** and that of the Ni(II) and Zn(II) complexes have been studied. It is shown that the solid-state structures are different for the two complexes: the Ni(II) metal ion adopts a N₄O₂ *pseudo*-octahedral coordination environment with the two tridentate HL⁻ ligands meridionally coordinated in a perfect orthogonal fashion, while the Zn(II) center lies in a N₃O₂ distorted trigonal bipyramidal geometry. The presence of several intermolecular contacts, including hydrogen bonds and $\pi \cdots \pi$ stacking interactions were visually gained by Hirshfeld Surface analysis. 2D fingerprint plots provided an estimation of the influence of such interactions on the crystal lattice and stability. Magnetic measurements showed high spin Co(II) ($S = 3/2$), Ni(II) ($S = 1$) and Cu(II) ($S = 1/2$) isolated spins at room temperature with no interaction between magnetic centers on cooling. The synthetic versatility and simplicity of the approach, allowing a facile scale-up of the procedure, depicted here suggest application in the chemical design of selective molecular scaffolds for multi-centered binding and reactivity.

Experimental Section

General considerations: Reactions were performed under nitrogen atmosphere using standard Schlenk techniques. The solvents were dried and distilled according to standard procedures.^[68] 8-hydroxy-2-quinolinecarboxaldehyde, 2-aminophenol, nickel(II) acetate tetrahydrate, copper(II) acetate hydrate, cobalt(II) acetate tetrahydrate and zinc(II) acetate dihydrate were purchased from commercial sources and used without further purification. Infrared spectra were recorded on a Nicolet Magna 550, FT-IR spectrophotometer, as KBr disks in the 4000 to 400 cm⁻¹ range. ¹H and ¹³C NMR spectra were recorded on a Bruker Avance 400 Digital Instrument. All NMR spectra are reported in parts per million (ppm, δ) relative to tetramethylsilane (Me₄Si), with the residual solvent proton and carbon resonances used as internal standards. The following abbreviations are used to describe peak patterns: br, broad; s, singlet; t, triplet and m, multiplet. High resolution electrospray ionization mass spectra (ESI-MS) were conducted on a Bruker MAXI 4G mass spectrometer in positive mode, at the Centre Régional de Mesures Physiques de l'Ouest (CRMPO, Université de Rennes 1, France). Elemental analyses were conducted on a Thermo-Finnigan Flash EA 1112 CHNS/O analyzer by the Microanalytical Service of the CRMPO. The temperature dependences of the

magnetizations for powdered samples have been measured with a SQUID magnetometer (Quantum design MPMS-XL5) operating between 2 and 300 K at a constant field of 2 kOe below 20 K and 10 kOe above, and diamagnetic corrections were applied by using Pascal's constants.^[69] Melting points were determined in evacuated capillaries on a Kofler Bristoline melting point apparatus and were not corrected.

Synthesis of the diprotic Schiff base precursor H_2L :^[54] A three-necked round bottom flask equipped with a Dean-Stark apparatus was loaded with a magnetic stir bar, 8-hydroxy-2-quinolinecarboxaldehyde (0.500 g, 2.89 mmol), 2-aminophenol (0.315 g, 2.89 mmol) and 15 mL of toluene. The reaction mixture was refluxed for 1 h. Then, the reaction was cooled at room temp. giving a microcrystalline yellow solid. The compound was collected by filtration, washed with 3 x 5 mL portion of cold MeOH, and dried under vacuum. Slow evaporation (7 days) of a dichloromethane solution yielded yellow single crystals of H_2L (0.415 g, 1.57 mmol, 83%). A suitable crystal from this crop was used for X-ray structure determination. M.p. 180-183 °C. IR (KBr): $\bar{\nu}$ = 3413(s) and 3363(s) (O-H), 3062(w) (C-H aryl), 1616(w), 1576(m), 1508(s) (C \equiv N) and (C \equiv C), 1465(s) (O-H), 1284(w) (C-O), 752(s) (C-H) cm^{-1} . 1H NMR (400 MHz, CD_3OD ; 315 K): δ = 10.21 (br s, 1 H, OH), 9.00 (s, 1 H, N=CH), 8.42 (t, 1 H, C_3H_2N), 8.36 (t, 1 H, C_3H_2N), 8.03 (br s, 1 H, OH), 7.52 (t, 1 H, C_6H_4), 7.42 (m, 1 H, C_6H_3), 7.40 (m, 1 H, C_6H_3), 7.18 (m, 2 H, C_6H_4), 6.96 (m, 2 H, $C_6H_4 + C_6H_3$) ppm. $^{13}C\{^1H\}$ NMR (101 MHz, $(CD_3)_2SO$, 298 K): δ = 155.9 (N=CH), 155.0 (C_{quat} , $C_3H_2N-CH=$), 153.9 ($(C_{quat}$, $C_6H_3-OH)$), 153.3 (C_{quat} , C_6H_4-OH), 139.8 (C_{quat} , C_6H_4-N), 138.1(C_{quat} , C_6H_3), 137.6 (CH, C_3H_2N), 131.0 (C_{quat} , C_6H_3), 129.7 (CH, C_6H_4), 129.6 (CH, C_6H_4), 120.8 (CH, C_6H_4), 120.7 (2 CH, $C_6H_4 + C_6H_3$), 119.8 (CH, C_6H_3) ppm. $C_{16}H_{12}N_2O_2$ calcd. C 72.72, H 4.58, N 10.60; found C 72.56, H 4.44, N 10.27.

Synthesis of complex $Co(HL)_2$ (1**):** A Schlenk tube was charged with a magnetic stir bar, H_2L (0.15 g, 0.57 mmol), cobalt(II) acetate tetrahydrate (0.70 g, 0.28 mmol) and 10 mL of MeOH. After 5 min of stirring, the reaction mixture was refluxed for 1.5 h. The reaction was cooled to room temp. giving a dark red precipitate. The solid material was filtered off, washed with 3 x 3 mL portion of cold MeOH, diethyl ether (2 x 3 mL portion), and dried under vacuum for 2 h, to afford **1** (0.76 g, 84%). M.p. 170-172 °C. IR (KBr): $\bar{\nu}$ = 3399 (br,m) (O-H), 3050(w) (C-H aryl), 1587(m) and 1498(w) (C \equiv N) and (C \equiv C), 1448(s) (O-H), 1277(w) (C-O), 754(s) (C-H) cm^{-1} . ESI-MS [m/z], calcd. $C_{32}H_{22}N_4O_4NaCo$: 608.08707, found: 608.0866 (0 ppm) $[M+Na]^+$. $C_{32}H_{22}N_4CoO_4 \cdot 2H_2O$ calcd. C 61.71, H 4.24, N 9.01; found C 61.98, H 3.81, N, 8.81.

Synthesis of complex Ni(HL)₂ (2): The synthesis of this complex was carried out following a procedure similar to that described for complex **1**, using, in this case, **H₂L** (0.100 g, 0.38 mmol), nickel(II) acetate tetrahydrate (0.047 g, 0.19 mmol) and 10 mL of MeOH. Recrystallization from vapor diffusion of diethyl ether into a methanol solution of the compound for 7 days provided red microcrystals of **2** (0.041 g, 67%). A suitable crystal from this crop was used for X-ray structure determination. M.p. 168-170 °C. IR (KBr): $\bar{\nu}$ = 3371(m) (O-H), 3049(w) (C-H aryl), 1585(m) and 1498(w) (C≡N) and ν (C≡C), 1448(s) (O-H), 1269(w) (C-O), 750(s) (C-H) cm⁻¹. ESI-MS (*m/z*), calcd for C₃₂H₂₃N₄O₄⁵⁸Ni: 585.10672, found: 585.1069 (0 ppm) [M+H]⁺. C₃₂H₂₂N₄NiO₄·H₂O calcd. C 63.71, H 4.01, N 9.29; found C 63.69, H 3.95, N 9.18.

Synthesis of complex Cu(HL)₂ (3): The synthesis of this dark orange complex was carried out following a procedure similar to that described for complex **1**, using, in this case, **H₂L** (0.15 g, 0.57 mmol), copper(II) acetate monohydrate (0.058 g, 0.29 mmol) and 10 mL of MeOH. (0.056 g, 60%). M.p. 168-170 °C. IR (KBr): $\bar{\nu}$ = 3367(w) (O-H), 3028(w) (C-H aryl), 1589(w) and 1552(m) (C≡N) and (C≡C), 1450(s) (O-H), 1238(m) (C-O), 744(s) (C-H) cm⁻¹. ESI-MS [*m/z*], calcd. C₃₂H₂₃N₄O₄⁶³Cu: 590.10153, found: 590.1012 (0 ppm) [M+H]⁺. C₃₂H₂₂N₄CuO₄ calcd. C 65.13, H 3.76, N 9.49; found C 64.93, H 3.70, N 9.53.

Synthesis of complex Zn(HL)₂ (4): The synthesis of this complex was carried out following a procedure similar to that described for complex **1**, using, in this case, **H₂L** (0.15 g, 0.57 mmol), zinc(II) acetate dihydrate (0.064 g, 0.29 mmol) and 10 mL of MeOH. Recrystallization from vapor diffusion of diethyl ether into a chloroform/dichloromethane solution mixture of the compound for 7 days afforded red microcrystals of **4** (0.075 g, 79%). A suitable crystal from this crop was used for X-ray structure determination. M.p. 168-170 °C. IR (KBr): $\bar{\nu}$ = 3375(w) (O-H), 3055(w) (C-H aryl), 1589(m) and 1494(m) (C≡N) and (C≡C), 1448(s) (O-H), 1278(m) (C-O), 750(s) (C-H) cm⁻¹. ¹H NMR (400 MHz, (CD₃)₂SO, 298 K): δ = 8.70 (s, 2 H, OH), 8.57 (m, 2 H, C₃H₂N), 7.65 (m, 4 H, C₃H₂N + C₆H₃), 6.62 (m, 2 H, C₆H₄), 6.48 (s, 2 H, CH=N), 6.26 (m, 2 H, C₆H₄), 6.20 (m, 2 H, C₆H₄), 6.00 (m, 4 H, C₆H₄ + C₆H₃), 5.96 (m, 2 H, C₆H₃) ppm. ¹³C{¹H} NMR (100 MHz, (CD₃)₂SO, 298 K): δ = 162.6 (C-O-Zn), 158.1 (CH=N), 152.3 (C-OH), 149.1 (CN, N-C₆H₄-2-OH), 139.5 (C_{quat}, C₆H₃), 138.5 (CH, C₆H₃), 136.7 (C_{quat}, C₃H₂N), 130.3 (C_{quat}, C₆H₃), 131.1, 128.7 (CH, N-C₆H₄-2-OH), 119.7 (CH, C₃H₂N), 119.2 (CH, C₆H₃), 118.6 (CH, C(H)=N), 116.3 (CH, C₆H₃), 112.5, 110.0 (CH, N-C₆H₄-2-OH) ppm. ESI-MS [*m/z*], calcd. C₃₂H₂₂N₄O₄Na⁶⁴Zn: 613.08302, found: 613.0830 (1 ppm) [M+Na]⁺. C₃₂H₂₂N₄O₄Zn·0.75H₂O calcd. C 63.47, H 3.92, N 9.26; found C 63.58, H 3.70, N 8.75.

X-ray crystal structure determination: A well-shaped crystal of each compound **H₂L**, **2** and **4** was coated in Paratone-N oil, mounted on a Kapton loop and transferred to the cold gas stream of the cooling device. Intensity data were collected at 150(2) K on a D8 VENTURE Bruker-AXS diffractometer equipped with a multilayer monochromated Mo-K α radiation ($\lambda = 0.71073 \text{ \AA}$) and a CMOS Photon100 detector. The three structures were solved by dual-space algorithm using the SHELXT program,^[70] and then refined with full-matrix least-square method based on F^2 (SHELXL-2014).^[71] All non-hydrogen atoms were refined with anisotropic atomic displacement parameters. Except oxygen linked hydrogen atoms that were introduced in the structural model through Fourier difference maps analysis, all H atoms were finally included in their calculated positions. In addition, the contribution of the disordered solvents to the calculated structure factors of **2** and **4** were estimated following the BYPASS algorithm,^[72] implemented as the SQUEEZE option in PLATON.^[73] Then, a new data set, free of solvent contribution, was used in the final refinement. Crystal data and details of data collection and refinement for **H₂L**, **2** and **4** are summarized in Table 4. ORTEP views were drawn using OLEX2 software.^[74] CCDC 1856459-1856461 contain the supplementary crystallographic data for this paper. These data can be obtained free of charge from The Cambridge Crystallographic Data Centre via www.ccdc.cam.ac.uk/data_request/cif

Table 4. Crystallographic data, details of data collection and structure refinement parameters for compounds **H₂L**, **2** and **4**.

	H₂L	2	4
Empirical Formula	C ₁₆ H ₁₂ N ₂ O ₂	C ₃₂ H ₂₂ N ₄ NiO ₄	C ₃₂ H ₂₂ N ₄ O ₄ Zn
Formula mass, g mol ⁻¹	264.28	585.24	591.90
Collection <i>T</i> , K	150(2)	150(2)	150(2)
Crystal size (mm)	0.58 x 0.09 x 0.04	0.31 x 0.16 x 0.08	0.08 x 0.05 x 0.015
Crystal color	Yellow	Black	Light brown
crystal system	Monoclinic	Triclinic	Monoclinic
space group	<i>P</i> 2 ₁	<i>P</i> -1	<i>P</i> 2 ₁ / <i>n</i>
<i>a</i> (Å)	11.930(5)	9.8744(10)	11.611(4)
<i>b</i> (Å)	4.4633(16)	11.4788(13)	15.595(5)
<i>c</i> (Å)	12.352(6)	14.6534(17)	16.306(5)
<i>α</i> (°)	90	111.161(4)	90
<i>β</i> (°)	106.526(17)	101.541(4)	107.960(10)
<i>γ</i> (°)	90	97.567(4)	90
<i>V</i> (Å ³)	630.5(5)	1479.3(3)	2808.6(16)
<i>Z</i>	2	2	4
<i>D</i> _{calcd} (g cm ⁻³)	1.392	1.314	1.400
F(000)	276	604	1216
abs coeff (mm ⁻¹)	0.094	0.698	0.919
<i>θ</i> range (°)	3.395 to 27.380	2.924 to 27.482	2.924 to 27.483
range <i>h,k,l</i>	-15/15, -5/5, -15/15	-12/11, -14/14, -19/18	-14/15, -20/18, -21/21
No. total refl.	4548	31658	28478
No. unique refl.	2723	6764	6414
Comp. <i>θ</i> _{max} (%)	98.5	99.9	99.7
Max/min transmission	0.996/0.840	0.946/0.838	0.986/0.829
Data/Restraints/Parameters	2723/2/187	6764/3/376	6414/0/372
Final <i>R</i>	<i>R</i> _I = 0.0822	<i>R</i> _I = 0.0354	<i>R</i> _I = 0.0789
[<i>I</i> > 2σ(<i>I</i>)]	<i>wR</i> ₂ = 0.1960	<i>wR</i> ₂ = 0.0782	<i>wR</i> ₂ = 0.1504
<i>R</i> indices (all data)	<i>R</i> _I = 0.1479 <i>wR</i> ₂ = 0.2382	<i>R</i> _I = 0.0506 <i>wR</i> ₂ = 0.0841	<i>R</i> _I = 0.2120 <i>wR</i> ₂ = 0.1963
Goodness of fit / <i>F</i> ²	1.052	1.021	0.992
Largest diff. Peak/hole (eÅ ⁻³)	0.574/-0.421	0.327/-0.352	0.973/-0.528

Hirshfeld Surface (HS) determination: The analyses of the surfaces were mapped using CrystalExplorer,^[75] starting from the crystallographic information file (CIF) of **H₂L**, **2** and **4**. The normalized contact distance (d_{norm}), defined in terms of d_e , d_i and the vdW radii of the atoms, was calculated using the Eq. 1, where the distance from the HS to the nearest nucleus internal (d_i) or external (d_e), with respect to the surface involved, and vdW is the van der Waals radii of atoms, according to the literature.^[65]

$$d_{norm} = \frac{d_i - r_i^{vdW}}{r_i^{vdW}} + \frac{d_e - r_e^{vdW}}{r_e^{vdW}} \quad \text{Eq. 1}$$

The dimensional (3D) HS maps are generated by d_{norm} , appears as a red spots over surfaces given a close-contact interactions, responsible of molecular packing in the crystal lattice. Also, 3D d_{norm} surfaces can be plotted in 2D fingerprint representations, to quantitatively summarize, the nature and the type of all intermolecular interactions present in each crystal packing. HS for **H₂L** and its complexes **2** and **4**, mapped over d_{norm} (range -0.76 to 2.38Å), are illustrated in Figure 5.

Acknowledgements

The authors thank Drs. F. Lambert and P. Jehan (CRMPO, Rennes) for helpful assistance with HR-MS measurements. Financial support from the Fondo Nacional de Desarrollo Científico y Tecnológico [FONDECYT (Chile), grant No. 11160658 (IR: N.N.)] and the Vicerrectoría de Investigación y Desarrollo, Universidad de Concepción (Chile), grant VRID Iniciación No. 216.021.034-10-1.0IN (IR: N.N.), the Centre National de la Recherche Scientifique (CNRS), the Université de Rennes 1, and the Chilean-French International Associated Laboratory for “Multifunctional Molecules and Materials” (LIAM3-CNRS N°1207) is gratefully acknowledged.

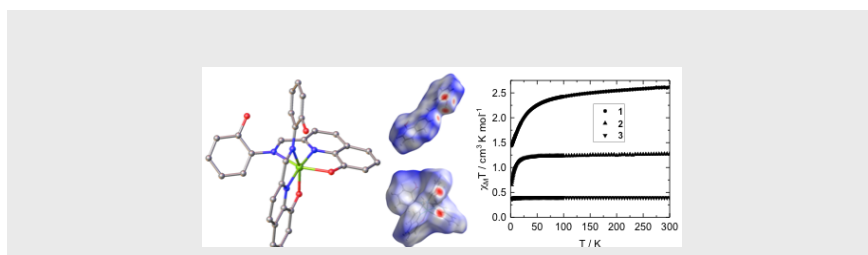
Keywords: ONN ligands; Schiff bases; Homoleptic Complexes; X-ray diffraction; Hirshfeld Surface Analysis.

- [1] R. Hernandez-Molina, A. Mederos, "Acyclic and Macrocyclic Schiff Base Ligands" in *Comprehensive Coordination Chemistry II* (Eds.: J. A. McCleverty, T. J. Meyer), Elsevier Pergamon, Oxford, **2004**, vol. 1, p. 411-458.
- [2] E. L. Gavey, M. Pilkington, *Coord. Chem. Rev.* **2015**, 296, 125.
- [3] M. Andruh, *Dalton Trans.* **2015**, 44, 16633.
- [4] H. L.C. Feltham, S. Brooker, *Coord. Chem. Rev.* **2009**, 253, 1458.
- [5] N. E. Borisova, M. D. Reshetova, Y. A. Ustynyuk, *Chem. Rev.* **2007**, 107, 46.
- [6] W. Radecka-Paryzek, V. Patroniak, J. Lisowski, *Coord. Chem. Rev.* **2005**, 249, 2156.
- [7] X. Liu, C. Manzur, N. Novoa, S. Celedon, D. Carrillo, J.-R. Hamon, *Coord. Chem. Rev.* **2018**, 357, 144.
- [8] J. Yang, R. Shi, P. Zhou, Q. Qiu, H. Li, *J. Mol. Struct.* **2016**, 1106, 242.
- [9] P. Das, W. Linert, *Coord. Chem. Rev.* **2016**, 311, 1.
- [10] X.-B. Lu, D. J. Darensbourg, *Chem. Soc. Rev.* **2012**, 41, 1462.
- [11] E. M. McGarrigle, D. G. Gilheany, *Chem. Rev.* **2005**, 105, 1563.
- [12] K.C. Gupta, A. K. Sutar, *Coord. Chem. Rev.* **2008**, 252, 1420.
- [13] J.-P. Costes, C. Duhayon, L. Vendier, A. J. Mota, *New J. Chem.* **2018**, 42, 3683.
- [14] C. Adhikary, S. Koner, *Coord. Chem. Rev.* **2010**, 254, 2933.
- [15] B. Weber, *Coord. Chem. Rev.* 2009, 253, 2432.
- [16] A. Dalla Cort, P. De Bernardin, G. Forte, F. Yafteh Mihan, *Chem. Soc. Rev.* **2010**, 39, 3863.
- [17] T. J. Boyle, J. M. Sears, J. A. Greathouse, D. Perales, R. Cramer, O. Staples, A. L. Rheingold, E. N. Coker, T. M. Roper, R. A. Kemp, *Inorg. Chem.* **2018**, 57, 2402.
- [18] X. Yang, R. A. Jones, S. Huang, *Coord. Chem. Rev.* **2014**, 273-274, 63.
- [19] C. R. Nayar, R. Ravikumar, *J. Coord. Chem.* **2014**, 67, 1.
- [20] R. M. Clarke, K. Herasymchuk, T. Storr, *Coord. Chem. Rev.* **2018**, 355, 180.
- [21] R. W.-Y. Sun, C.-M. Che, *Coord. Chem. Rev.* **2009**, 253, 1682.
- [22] R.-K. Lin, C.-I. Chiu, C.-H. Hsu, Y.-J. Lai, P. Venkatesan, P.-H. Huang, P.-S. Lai, C.-C. Lin, *Chem. Eur. J.* **2018**, 24, 4111.
- [23] P. Pfeiffer, E. Breith, E. Lubbe, T. Tsumaki, *Justus Liebigs Ann. Chem.* **1933**, 503, 84.
- [24] K. Gutierrez, J. Corchado, S. Lin, Z. Chen, D. M. Piñero Cruz, *Inorg. Chim. Acta* **2018**, 474, 118.
- [25] H. Naeimi, J. Safari, A. Heidarneshad, *Dyes and Pigments* **2007**, 73, 251.

- [26] J.-P. Costes, G. Cros, M. H. Darbieu, J.-P. Laurent, *Inorg. Chim. Acta* **1982**, *60*, 111.
- [27] S. Celedon, M. Fuentealba, T. Roisnel, J.-R. Hamon, D. Carrillo, C. Manzur, *Inorg. Chim. Acta* **2012**, *390*, 184.
- [28] R. C. Elder, *Aust. J. Chem.* **1978**, *31*, 35.
- [29] L. Rigamonti, A. Forni, M. Sironi, A. Ponti, A. M. Ferretti, C. Baschieri, A. Pasini, *Polyhedron* **2018**, *145*, 22.
- [30] N. Novoa, T. Roisnel, V. Dorcet, O. Cador, C. Manzur, D. Carrillo, J.-R. Hamon, *New J. Chem.* **2016**, *40*, 5920, and references cited therein.
- [31] S. Kumari, A. K. Mahato, A. Maurya, V. K. Singh, N. Kesharwani, P. Kachhap, I. O. Koshevoy, C. Haldar, *New J. Chem.* **2017**, *41*, 13625.
- [32] Y. Min Byun, J. Min Lee, J. Yeon Ryu, M. Jeong Go, K. Su Na, Y. Kim, J. Lee, *Polyhedron* **2018**, *141*, 191.
- [33] T. Basak, K. Ghosh, S. Chattopadhyay, *Polyhedron* **2018**, *146*, 81.
- [34] Z.-P. Qi, J.-J. Sun, L.-L. Zhu, H. Zhang, *Polyhedron* **2014**, *81*, 646.
- [35] P. Bhowmik, L. Kanta Das, A. Bauzá, S. Chattopadhyay, A. Frontera, A. Ghosh, *Inorg. Chim. Acta* **2016**, *448*, 26.
- [36] I. Buta, L. Cseh, C. Cretu, D. Aparaschivei, C. Maxim, P. Lönnecke, E. Hey-Hawkins, N. Stanica, E. Ohler, E. Rentschler, M. Andruh, O. Costisor, *Inorg. Chim. Acta* **2018**, *475*, 133.
- [37] M. Andruh, *Chem. Commun.* **2011**, *47*, 3025.
- [38] B. Mynster-Dahl, O. Dahl, *Acta Chem. Scand.* **1969**, *23*, 1503.
- [39] J. Sirirak, W. Phonsri, D.J. Harding, P. Harding, P. Phommon, W. Chaoprasa, R.M. Hendry, T.M. Roseveare, H. Adams, *J. Mol. Struct.* **2013**, *1036*, 439.
- [40] T. Thirunavukkarasu, H. A. Sparkes, K. Natarajan, V. G. Gnanasoundari, *Inorg. Chim. Acta* **2018**, *473*, 255.
- [41] A. Hens, P. Mondal, K. K. Rajak, *Dalton Trans.* **2013**, *42*, 14905.
- [42] P. Ghorai, P. Brandão, A. Bauzá, A. Frontera, A. Saha, *Inorg. Chim. Acta* **2018**, *469*, 189.
- [43] W. Phonsri, D. S. Macedo, C. G. Davies, G. N. L. Jameson, B. Moubaraki, K. S. Murray, *Dalton Trans.* **2017**, *46*, 7020.
- [44] J.-P. Zhao, Y. Xie, J.-R. Li, *Dalton Trans.* **2016**, *45*, 1514.
- [45] P. Insiti, P. Jitthiang, P. Harding, K. Chainok, R. Chotima, J. Sirirak, S. Blackwood, A. Alkas, S. G. Telfer, D. J. Harding, *Polyhedron* **2016**, *114*, 242.

- [46] P. Ghorai, A. Chakraborty, A. Panja, T. K. Mondal, A. Saha, *RSC Adv.* **2016**, *6*, 36020.
- [47] P. K. Bhaumik, A. Bauzá, M. G. B. Drew, A. Frontera, S. Chattopadhyay, *CrystEngComm* **2015**, *17*, 5664.
- [48] S. Nayak, P. Gamez, B. Kozlevčar, A. Pevec, O. Roubeau, S. Dehnen, J. Reedijk, *Polyhedron* **2010**, *29*, 2291.
- [49] M. Shyamal, T. K. Mandal, A. Panja, A. Saha, *RSC Adv.* **2014**, *4*, 53520.
- [50] A. B. Pradhan, S. K. Mandal, S. Banerjee, A. Mukherjee, S. Das, A. R. Khuda Bukhsh, A. Saha, *Polyhedron* **2015**, *94*, 75.
- [51] S. Nayak, A. Pevec, C. C. Seaton, P. Gamez, J. Reedijk, *Polyhedron* **2016**, *107*, 172.
- [52] H.-L. Gao, S.-X. Huang, X.-P. Zhou, Z. Liu, J.-Z. Cui, *Dalton Trans.* **2018**, *47*, 3503.
- [53] H.-L. Gao, L. Jiang, S. Liu, H.-Y. Shen, W.-M. Wang, J.-Z. Cui, *Dalton Trans.* **2016**, *45*, 253.
- [54] T. Hata, T. Uno, *Bull. Chem. Soc. Jpn.* **1972**, *45*, 477.
- [55] P. Zabierowski, J. Szklarzewicz, K. Kurpiewska, K. Lewinski, W. Nitek, *Polyhedron* **2013**, *49*, 74.
- [56] O. Stetsiuk, S. R. Petrusenko, A. El-Ghayoury, V. N. Kokozay, N. Avarvari, *Inorg. Chim. Acta* **2018**, *475*, 172.
- [57] P. K. Suganthy, R. N. Prabhu, V. S. Sridevi, *Inorg. Chim. Acta* **2016**, *449*, 127.
- [58] N. Novoa, V. Dorcet, S. Sinbandhit, C. Manzur, D. Carrillo, J.-R. Hamon, *J. Coord. Chem.* **2014**, *67*, 4101.
- [59] M. A. Al-Anber, *Am. J. Phys. Chem.* **2013**, *2*, 1.
- [60] A. Trujillo, M. Fuentealba, D. Carrillo, C. Manzur, I. Ledoux-Rak, J.-R. Hamon, J.-Y. Saillard, *Inorg. Chem.* **2010**, *49*, 2750.
- [61] S. Celedón, M. Fuentealba, T. Roisnel, I. Ledoux-Rak, J.-R. Hamon, D. Carrillo, C. Manzur, *Eur. J. Inorg. Chem.* **2016**, 3012.
- [62] J. Cisterna, V. Artigas, M. Fuentealba, P. Hamon, C. Manzur, J.-R. Hamon, D. Carrillo, *Inorganics*, **2018**, *6*, 5.
- [63] L. Rigamonti and A. Forni, *Inorg. Chim. Acta* **2018**, *473*, 216.
- [64] S. Bhattacharyya, S. B. Kumar, S. K. Dutta, E. R. T. Tiekink, M. Chaudhury, *Inorg. Chem.* **1996**, *35*, 1967.
- [65] M. Spackman, D. Jayatilaka, *CrystEngComm* **2009**, *11*, 19.

- [66] O. Kahn, *Molecular Magnetism*, VCH Publishers, New York, **1993**.
- [67] L. Rigamonti, N. Bridonneau, G. Poneti, L. Tesi, L. Sorace, D. Pinkowicz, J. Jover, E. Ruiz, R. Sessoli, A. Cornia, *Chem. Eur. J.* **2018**, *24*, 8857-8868.
- [68] W. L. F. Armarego, C. L. L. Chai, *Purification of Laboratory Chemicals*, Fifth ed., Butterworth-Heinemann, Elsevier Inc., Amsterdam, The Netherlands, **2003**.
- [69] P. Pascal, *Ann. Chim. Phys.* **1910**, *19*, 5.
- [70] G. M. Sheldrick, *Acta Crystallogr., Sect. A* **2015**, *71*, 3.
- [71] G. M. Sheldrick, *Acta Crystallogr., Sect. C* **2015**, *71*, 3.
- [72] P. Van Der Sluis, A. L. Spek, *Acta Crystallogr., Sect. A* **1990**, *46*, 194.
- [73] A. L. Spek, *J. Appl. Crystallogr.* **2003**, *36*, 7.
- [74] O. V. Dolomanov, L. J. Bourhis, R. J. Gildea, J. A. K. Howard, H. Puschmann, *J. Appl. Crystallogr.* **2009**, *42*, 339.
- [75] M. J. Turner, J. J. McKinnon, S. K. Wolff, D. J. Grimwood, P. R. Spackman, D. Jayatilaka, M. A. Spackman, *CrystalExplorer17*, University of Western Australia, **2017**.



Four transition metal complexes bearing a O,N,N-donor 8-hydroxyquinoline Schiff base ligand were efficiently synthesized, and their spectroscopic, structural, Hirshfeld surface and magnetic properties have been investigated.

Homoleptic Schiff base Complexes, Hirshfeld Surface Analysis

Déborah González, Ramón Arrué, Edison Matamala-Cea, Rodrigo Arancibia, Paul Hamon, Olivier Cador, Thierry Roisnel, Jean-René Hamon and Néstor Novoa**

Page No. – Page No.

Homoleptic Co(II), Ni(II), Cu(II), and Zn(II) complexes based on 8-hydroxyquinoline Schiff base derivative: a combined synthetic, spectral, structural, and magnetic study